nature nanotechnology

SUPPLEMENTARY INFORMATION

DOI: 10.1038/NNANO.2016.171

Direct observation of the layer-dependent electronic structure in phosphorene

Likai Li, Jonghwan Kim, Chenhao Jin, Guojun Ye, Diana Y. Qiu, Felipe H. da Jornada, Zhiwen Shi, Long Chen, Zuocheng Zhang, Fangyuan Yang, Kenji Watanabe, Takashi Taniguchi, Wencai Ren, Steven G. Louie*, Xianhui Chen*, Yuanbo Zhang* and Feng Wang*

* Email: fengwang76@berkeley.edu; zhyb@fudan.edu.cn; chenxh@ustc.edu.cn, sglouie@berkeley.edu

DOI: 10.1038/NNANO.2016.171

S1. Estimation of sample thickness: optical contrast and AFM measurement

We combined optical contrast and atomic force microscopy (AFM) measurements to estimate the layer-number of the few-layer black phosphorus (BP) flakes. Accurate thickness determination for isolated phosphorene flakes is difficult using AFM due to the different tip-surface interaction on phosphorene and SiO_2/Si wafer. However, the AFM height difference between two adjacent flakes of different thickness can yield useful information, since an average height increase of 0.5 nm is expected for one additional atomic layer. Indeed, for monolayer terraces on a black phosphorus flake, an average AFM height difference was found to be ~ 0.5 nm, which is consistent with the thickness of monolayer black phosphorus (Figure S1b and S1c). Meanwhile, the optical contrast $\left(1-\left(\frac{R_{sample}}{R_{substrate}}\right)\right.$, where R_{sample} and $R_{substrate}$ are the reflectance of the sample flake and the Si wafer with 300 nm thermally growth SiO_2 layer, respectively) of the red channel of the CCD image shows a difference of ~ 7% (Fig. 1d in the main text). We could therefore use such contrast to estimate the layer-number of the few-layer phosphorene flakes. Such estimation was later verified by the layer-dependent optical absorption resonances, as described in the main text.

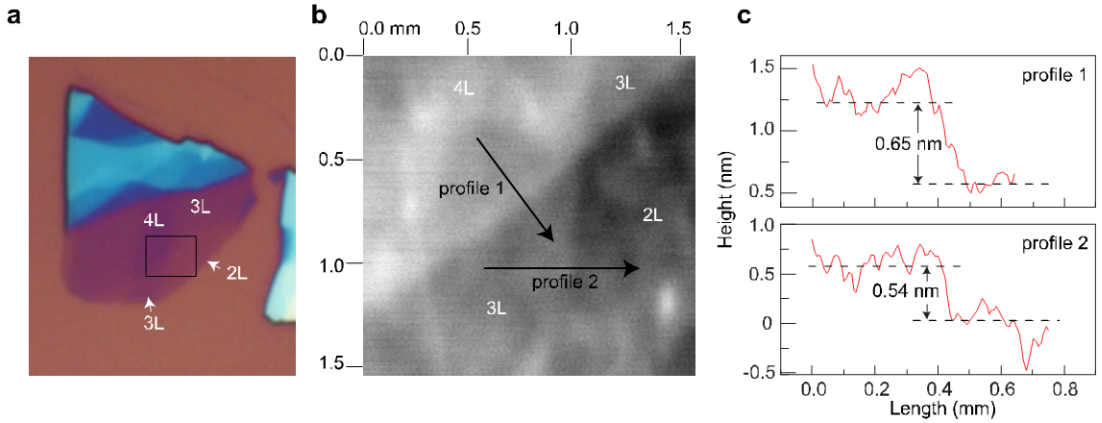

Figure S1 | Preliminary estimation of sample thickness. a, Optical image of bilayer, trilayer and tetralayer phosphorene samples on Si wafer with 300 nm thermally growth SiO_2 layer. The image was recorded with a CCD camera attached to an optical microscope. **b**, AFM image of the sample area marked in **a**. **c**, AFM height profiles measured along line-cuts shown in **b**. An average height difference of ~ 0.5 nm is obtained on monolayer terraces.

S2. Obtaining absorption resonances from the reflectance spectra

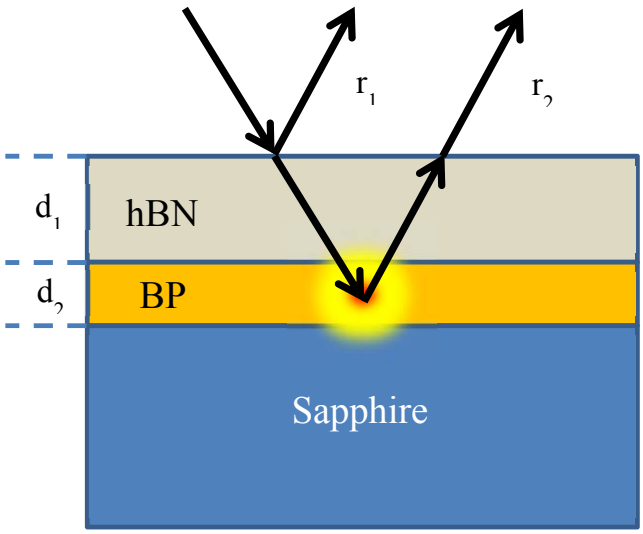

Figure S2. Illustration of light reflection from the hBN-BP-sapphire system. The normal incident light is drawn obliquely for visual clarity.

The phosphorene samples are encapsulated between sapphire substrate and hexagonal boron nitride (hBN). The difference spectrum ΔR/R from phosphorene is related to its complex dielectric constant through Fresnel equation with known refractive indices of hBN and sapphire and the hBN thickness.

In the visible and near-infrared spectral region, the refractive index of hBN and sapphire can be approximated as a constant with $n_{BN} = n_{Sapphire} = 1.75$ (denoted as n_1). The hBN thickness (d_1) is approximately 15 nm in our devices. We denote the phosphorene dielectric constant and effective thickness as $\varepsilon_2(\omega)$ and d_2, respectively.

Optical reflection changes from atomically thin layers such as phosphorene can be treated as a small perturbation, and it has the form of $\frac{\Delta R}{R} = -Re[\sigma \cdot c_l^2/c_r]$ (Refs. 1,2). , where c_l is the local field factor at the sample, c_r is the reflection coefficient, and $\sigma = \frac{\omega d_2}{i}(\varepsilon_2 - 1)$ is the two-dimensional optical conductivity of black phosphorous. The reflection is dominated by the hBN-air interface r_1 as shown in Fig. S2, therefore $c_r = r_1 = \frac{n_0 - n_1}{n_0 + n_1}$. The local electric field at sample has the form $c_l = t_1 e^{i\varphi}$. Here $t_1 = \frac{2n_0}{n_0 + n_1}$ is the transmission from air to hBN, and $\varphi = 2\pi \frac{n_1 \omega d_1}{c_0}$ is the phase change of light propagating through the hBN layer. The final result is.

DOI: 10.1038/NNANO.2016.171

$$\frac{\Delta R}{R} = \frac{4\omega d_2}{n_1^2 - 1}\mathrm{Im}\left[(\varepsilon_2 - 1)e^{i2\varphi}\right] = \frac{4\omega d_2}{n_1^2 - 1}\mathrm{Im}\left[(\varepsilon_2 - 1)e^{i\frac{4\pi\omega d_1}{c_0}}\right] \quad \text{(S1)}$$

If the hBN thickness is negligible (*i.e.* $e^{i\varphi} = 1$), the reflectance contrast is proportional to the imaginary part of ε_2 (*i.e.* optical absorption). However, the finite hBN thickness makes $e^{i\varphi}$ complex; thus both real and imaginary part of ε_2 will contribute to the reflectance contrast. Eq. S1 shows that the contribution from real part of ε_2 increases with light frequency. This contribution from the real part of ε_2 accounts for the broad background observed in our reflectance spectra, and it is present for both polarizations. The optical resonances, however, is dominated by the imaginary part of ε_2 (*i.e* optical absorption from phosphorene). Quantitative evaluation of Eq. S1 shows that we can determine the optical absorption resonance energies from the reflection peaks with an uncertainty less than 25 meV.

S3. Phenomenological tight binding model of few-layer phosphorene

Since the direct bandgap is at the Γ point in N-layer phosphorene, we only need to consider the coupling among the N CBM (or VBM) states at the Γ point, with one state from each layer. In this scheme, the N-layer phosphorene is equivalent to a finite 1D lattice (or an linear molecule) of N identical atoms with only nearest-neighbor coupling. Assuming that, for an isolated monolayer phosphorene, the CBM (VBM) state at the Γ point has an energy $+\frac{E_{g0}}{2}(-\frac{E_{g0}}{2})$, and the coupling between neighboring layers is $\gamma^c(\gamma^v)$, the 1D lattice will then compose of N atoms with energy $+\frac{E_{g0}}{2}(-\frac{E_{g0}}{2})$ and nearest neighbor hopping $\gamma^c(\gamma^v)$. The Hamiltonian of this 1D lattice model reads:

$$H_N = \sum_{j=1}^{N} \pm\frac{E_{g0}}{2}C_j^+C_j + (\sum_{j=1}^{N-1}\gamma^{(s)}C_{j+1}^+C_j + \text{h.c.}) \quad \text{(S2)}$$

where $(s) = c, v$ stands for conduction and valence band, C_j^+/C_j $(j = 1 \ldots N)$ is the creation/annihilation operator on j^{th} atom (i.e. j^{th} layer), $C_j^+|0\rangle = |\phi_j\rangle$ is the state from j^{th} atom (i.e. j^{th} layer). The eigen wavefunction of the Hamiltonian can be generally written as $|\psi\rangle = \sum_{j=1}^{N} a^j |\phi_j\rangle$, which has a clear physical meaning that the eigen wavefucntion $|\psi\rangle$ of N layer BP have contribution from each layer; and that the coefficient a^j contains full information of how the different layers are mixed.

The eigenenergy and wavefunction of Eq. S2 can be solved by directly diagonalizing the N by N tridiagonal matrix. Alternatively, here we will use a simpler and more intuitive approach, owing to analogy to the 1D lattice. An infinite 1D lattice supports a travelling wave, with eigen wavefunction $a^j = e^{ikj}$ and eigenenergy $E_k = \pm\frac{E_{g0}}{2} + 2\gamma^{(s)}cosk$. For a finite 1D lattice, the two atoms at the end have only one nearest neighbor, and the boundary condition is equivalent to having two additional fixed atoms on each end (*i.e* 0^{th} and $(\text{N+1})^{\text{th}}$ atoms with $a^0 = a^{N+1} = 0$). The finite 1D lattice of N+2 atoms with fixed ends can be easily solved, and the resulting n-th eigenwavefunction and eigenenergy can be described by

$$a_{N,n}^{j} = \sin\left(k_{N,n}j\right), k_{N,n} = \frac{N+1-n}{N+1}\pi, n = 1 \ldots N \qquad \text{(S3)}$$

$$E_{N,n}^{(s)} = \pm\frac{E_{g0}}{2} + 2\gamma^{(s)}cosk_{N,n} = \pm\frac{E_{g0}}{2} - 2\gamma^{(s)}cos\left(\frac{n}{N+1}\pi\right)$$

Here n indexes the conduction and valence subbands starting from the bandgap.

Modes with different n in Eq. S3 correspond to different orders of standing waves on the 1D lattice. Optical transitions are allowed only between two subbands with the same n for in-plane light polarizations. The transition energy between nth valence to nth conduction band is described by:

$$E_{N,n}^{R} = E_{g0} - 2(\gamma^{c} - \gamma^{v})\cos\left(\frac{n}{N+1}\pi\right) \qquad \text{(S4)}.$$

e.g. n = 1 corresponds to bandgap transitions, n = 2 and n = 3 describes the first and second above-bandgap resonances, respectively.

The model described above includes only the single lowest energy state from each layer. This approximation becomes less accurate for higher energy subbands, which can hybridize with other states not included in the model. Comparisons with *ab initio* calculations show that the simple tight-binding model provides a good approximation in 1-3 layer phosphorene, as well as low energy transitions in tetralayer phosphorene and thicker layers.

S4. Ab initio calculations

We first performed density functional theory (DFT) calculations in the generalized gradient approximation using the Quantum Espresso code [3]. We relaxed the geometry of one to four layer phosphorus in a supercell arrangement using a plane wave basis with norm conserving PBE [4] pseudopotentials with a van der Waals correction [5,6] and a 55 Ry wave function cutoff. A large vacuum was included between repeated supercells in the aperiodic direction so that 99% of the charge density was contained in half of each supercell.

The GW-Bethe-Salpeter equation (GW-BSE) calculation was done with the BerkeleyGW code [7–9]. We performed a one-shot GW calculation to obtain the quasiparticle (QP) bandstructure. The dynamical screening effects were accounted for with the Hybertsen-Louie generalized plasmon pole (HL-GPP) model [8]. We used a 14×10×1 *k*-grid to sample the Brillouin zone, included plane-wave components up to a cutoff of 15 Ry in the dielectric matrix, and included unoccupied states with energy up to 10 Ry to converge the QP energies to better than 0.1 eV. The static remainder technique was used to speed up convergence with respect to unoccupied states [10]. A truncated Coulomb interaction was used to prevent spurious interactions between periodic images [11]. We solved the BSE on an 80×96×1 *k*-grid, which converges the excitation energies to better than 0.1 eV, and included valence and conduction bands involved in transitions up to 3 eV.

To include the effect of the encapsulation, we first explicitly relaxed the distance between black phosphorene and 25 Å of sapphire and 25 Å of hexagonal boron nitride at the DFT level to

DOI: 10.1038/NNANO.2016.171

125 determine the distance between the substrate and the black phosphorus. We then included the
126 effect of screening from the sapphire substrate and boron nitride capping layer on the self-energy
127 and the electron-hole interaction following the method in Refs. 12,13.

128

129

130 **References**

131 1. Wang, F. *et al.* Gate-Variable Optical Transitions in Graphene. *Science* **320,** 206–209 (2008).

132 2. Mak, K. F. *et al.* Measurement of the Optical Conductivity of Graphene. *Phys. Rev. Lett.* **101,**
133 196405 (2008).

134 3. Giannozzi, P. *et al.* QUANTUM ESPRESSO: a modular and open-source software project
135 for quantum simulations of materials. *J. Phys. Condens. Matter* **21,** 395502 (2009).

136 4. Perdew, J. P., Burke, K. & Ernzerhof, M. Generalized Gradient Approximation Made Simple.
137 *Phys. Rev. Lett.* **77,** 3865–3868 (1996).

138 5. Grimme, S. Semiempirical GGA-type density functional constructed with a long-range
139 dispersion correction. *J. Comput. Chem.* **27,** 1787–1799 (2006).

140 6. Barone, V. *et al.* Role and effective treatment of dispersive forces in materials: Polyethylene
141 and graphite crystals as test cases. *J. Comput. Chem.* **30,** 934–939 (2009).

142 7. Deslippe, J. *et al.* BerkeleyGW: A massively parallel computer package for the calculation of
143 the quasiparticle and optical properties of materials and nanostructures. *Comput. Phys.*
144 *Commun.* **183,** 1269–1289 (2012).

145 8. Hybertsen, M. S. & Louie, S. G. Electron correlation in semiconductors and insulators: Band
146 gaps and quasiparticle energies. *Phys. Rev. B* **34,** 5390–5413 (1986).

147 9. Rohlfing, M. & Louie, S. G. Electron-hole excitations and optical spectra from first
148 principles. *Phys. Rev. B* **62,** 4927–4944 (2000).

10. Deslippe, J., Samsonidze, G., Jain, M., Cohen, M. L. & Louie, S. G. Coulomb-hole summations and energies for GW calculations with limited number of empty orbitals: A modified static remainder approach. *Phys. Rev. B* **87,** 165124 (2013).
11. Ismail-Beigi, S. Truncation of periodic image interactions for confined systems. *Phys. Rev. B* **73,** 233103 (2006).
12. Ugeda, M. M. *et al.* Giant bandgap renormalization and excitonic effects in a monolayer transition metal dichalcogenide semiconductor. *Nat. Mater.* **13,** 1091–1095 (2014).
13. Bradley, A. J. *et al.* Probing the Role of Interlayer Coupling and Coulomb Interactions on Electronic Structure in Few-Layer MoSe2 Nanostructures. *Nano Lett.* **15,** 2594–2599 (2015).